Simultaneous proton density, T1 , T2 , and flip-angle mapping of the brain at 7 T using multiparametric 3D SSFP imaging and parallel-transmission universal pulses

Lisa Leroi, Vincent Gras, Nicolas Boulant, Mathilde Ripart, Emilie Poirion, Mathieu D Santin, Romain Valabrègue, Franck Mauconduit, Lucie Hertz-pannier, Denis Le Bihan, et al.

Simultaneous PD, T_1, T_2 and flip angle mapping of the brain at 7T using multi-parametric 3D SSFP imaging and parallel transmission universal pulses

Lisa Leroi[1], Vincent Gras[1], Nicolas Boulant[1], Mathilde Ripart[1], Emilie Poirion[1,3], Mathieu D. Santin[2-3], Romain Valabregue[2-3], Franck Mauconduit[1], Lucie Hertz-Pannier[1], Denis Le Bihan[1], Ludovic de Rochefort[4†] and Alexandre Vignaud[1†]

[1] NeuroSpin, CEA, Paris-Saclay University, Gif-sur-Yvette, France ;
[2] CENIR, ICM, Hôpital Pitié-Salpêtrière, Paris, France;
[3] ICM, Inserm U 1127, CNRS UMR 7225, Sorbonne Universités, UPMC Université Paris 06 UMR S1127, Institut du Cerveau et de la Moelle épinière, Paris, France;
[4] CRMBM, UMR 7339, Aix-Marseille University, Marseille, France;

Corresponding author: Alexandre Vignaud, alexandre.vignaud@cea.fr

Word count: approx. 4887 words

Abstract:

Purpose: Performing simultaneous quantitative MRI at ultra-high field is challenging, as B_0 and B_1^+ heterogeneities as well as Specific Absorption Rate increase. Too large deviations of flip angle from the target can induce biases and impair signal-to-noise ratio in the quantification process. In this work, we use calibration-free parallel transmission, a dedicated pulse sequence parameter optimization and signal fitting to recover 3D proton density, flip angle, T_1 and T_2 maps over the whole brain, in a clinically suitable time.

Methods: Eleven optimized contrasts were acquired with an unbalanced Steady-State Free Precession sequence by varying flip angle amplitude and radiofrequency phase cycling increment, at a 1.0x1.0x3.0mm^3 resolution. Acquisition time was of 16min36sec for the whole brain. Parallel transmission and Universal Pulses were used to mitigate B_1^+ heterogeneity to improve the results' reliability over six healthy volunteers (3 females/males, age 22.6±2.7 years-old). Quantification of the physical parameters was performed by fitting acquired contrasts to the simulated ones using the Bloch-Torrey equations with a realistic diffusion coefficient.

Results: Whole-brain 3D maps of effective flip angle, PD and relaxation times were estimated. Parallel transmission improved the robustness of the results at 7T. Results were in accordance with literature and with measurements from standard methods.

Conclusion: These preliminary results show robust PD, FA, T_1 and T_2 map retrieval. Other parameters, such as Apparent Diffusion Coefficient, could be assessed. With further optimization in the acquisition, scan time could be reduced and spatial resolution increased to bring this multi-parametric quantification method to clinical research routine at 7-tesla.

Keywords : quantitative MRI, T1, T2, relaxometry, Parallel transmission, Universal Pulses

† These authors contributed equally to this work

Published as:
Leroi L, Gras V, Boulant N, Ripart M, Poirion E, Santin MD, Valabregue R, Mauconduit F, Hertz-Pannier L, Le Bihan D, de Rochefort L, Vignaud A. *Simultaneous proton density, T1 , T2 , and flip-angle mapping of the brain at 7 T using multiparametric 3D SSFP imaging and parallel-transmission universal pulses.*
Magn Reson Med 2020 Jul 3. doi: 10.1002/mrm.28391..

1. Introduction

In the vast majority of routine MRI investigations, contrast-weighted MR imaging techniques are used since they are fast enough to be compatible with a clinical workflow. The physicians establish their reports based on their expertise to interpret the links between a combination of weighted images and the underlying physiopathology. However, the retrieved signal is related to the acquisition parameters and to the different tissue properties in a complex way. It also depends on external factors that can hardly be reproduced over time, such as the patient positioning in the coil, leading to spatially heterogeneous contrasts influenced by both the B_1 transmit inhomogeneity and the coil receiving sensitivity, providing variable and hardly reproducible results. Quantifying directly the tissue physical properties T_1, T_2, and Proton Density (PD) would be helpful for the detection of both focal and diffuse pathologies thanks to their objective characterization. In addition, working with quantitative data allows comparing multi-centric MR data, and hence facilitates group comparisons (1). Abnormal relaxation time values have been reported in numerous contexts to improve the detection and staging of various diseases, e.g. in studies concerning autism, dementia, Parkinson's disease, multiple sclerosis, epilepsy or stroke (2).

One may expect that in many circumstances the combined measurement of complementary MR parameters during an exam would lead to a better diagnostic accuracy, but also to help interpret physiopathological events (3,4). The most straightforward approach is certainly to perform a sequential acquisition of the distinct parameters using different appropriate methods (5). However, by doing so, acquisition time can be very limiting. In addition, motion, interpolations and rescaling between acquisitions with various voxel size or bandwidths can render such approaches difficult (6). Another option is to perform a single type acquisition that is sensitive to all targeted MR parameters simultaneously, either in a transient or steady state, to retrieve multiple NMR parameters. Following this idea, several multi-parametric approaches have emerged in the literature. Non-exhaustively, in 2004, Schmitt et al.(7) proposed a method implementing an inversion pulse, followed by the acquisition of a train of balanced steady-state free precession (bSSFP) images. An analytical expression of the subsequent signal was proposed for the direct calculation of T_1, T_2, and relative PD. In Magnetic Resonance Fingerprinting (MRF), Ma et al. (8) enhanced this quantification strategy by undersampling bSSFP images and pseudo-randomizing the acquisition pattern by varying TR and flip angle (FA) simultaneously, such that each tissue generates a unique signal evolution to facilitate its identification from a dictionary. This MRF method has also been applied using spoiled SSFP patterns (9). An analogous approach called MR-STAT, in which the quantitative MR problem is treated as a dynamic system identification process in the time domain (10)

has also been proposed recently. Other multi-parametric strategies have been developed based on SSFP with Cartesian sampling such as QRAPTEST (6), using a saturation pulse and two echoes to characterize the signal relaxation parameters. Some alternative approaches can estimate multiple physical properties by using multiple echoes to obtain a complex signal dependency, such as Double-Echo Steady State (DESS)(11) or Triple Echo Steady-State(12). In particular, a method to perform Quantitative Imaging using Configuration States (QuICS), based on the acquisition of several SSFP images with different contrasts obtained by varying RF spoiling, FA, and/or spoiling gradient has been proposed (13,14) and successfully applied to assess in vitro sodium concentration, relaxivity and diffusivity(15). In such method, the acquired MR signal is sensitive to PD, T_1, T_2, FA and ADC, and can be modeled by the Bloch-Torrey equations. Therefore, with an appropriate choice for the acquired signal, it is possible to reconstruct the MR parameters from the QuICS contrasts through a straightforward fitting with the Bloch-Torrey equation.

In parallel, with the aim of continuously improving MRI and associated medical diagnosis, an upscaling trend to go towards Ultra-High Field (UHF), at 7 Tesla or higher, is observed. With higher signal-to-noise ratios (SNR), UHF Magnetic Resonance images provide unprecedented potential for clinical and neuroscientific research. Higher spatial resolutions become achievable, while maintaining acceptable scan time in the context of a patient examination (16–20). When it comes to quantitative MRI, UHF systems have the potential to increase the precision of the quantitative measurement and hence benefit greatly to clinical research field with e.g. the assessment of drug benefit or disease follow-up(21). Therefore, new quantitative imaging methods compatible with any magnetic field are now a major need. So far, multi-parametric qMRI have shown limitations at UHF, due to increased susceptibility effects and to radiofrequency (RF) field inhomogeneity. The major issue encountered in the parameters estimations is usually the complex dependency of the extraction to the effective FA, which can vary dramatically over the imaged volume at UHF, introducing the need of long and complex post-processing to overcome such issues (22). In addition, some of the presented approaches require large FA, not always achievable due to strong specific absorption rate (SAR) constraints. To homogenize prospectively the FA excitation, different solutions can be used. Dielectric shimming can be performed to locally enhance the B_1^+ field, near high permittivity materials (23) or meta-materials (24). To obtain a global FA map homogenization, K_T-points tailored pulses have been proposed as B_1^+ inhomogeneity mitigation candidate in 3D (25). Using this technique, the measurement of B_1^+ and ΔB_0 maps is necessary, and the pulse design must be performed "on the fly" during the exam. For a good FA homogeneity, pulses are usually of the order of several milliseconds, which can become prohibitive in qMRI because of the T_2 relaxation occurring during the pulse. Adding more transmission channels using parallel transmission (pTx) is usually favored in the MR

community as it yields a very good FA homogeneity with a shorter excitation time (of the order of 1 ms or less). But calibration time increases with the number of transmission channels and the pulse design must still be performed during the exam. It should also be noted that the performance of RF shimming is quite limited for 3D sequences. Recently, Gras et al. proposed a plug-and-play solution, called “Universal Pulses” (UP)(26). Such user-friendly scheme is able to mitigate efficiently the RF field inhomogeneity without B_1^+ and ΔB_0 measurements, while satisfying various hardware and safety constraints.

The aim of this work was to design a QuICS protocol and demonstrate its ability to perform simultaneous and robust NMR property quantitative extractions of PD, T_1 and T_2 on human brains in vivo at 7T in a clinically research viable time. To minimize the number of QuICS samples necessary for such an estimation, we developed an optimization algorithm based on the minimization of Cramer-Rao lower bounds, selecting the most appropriate set of acquisition parameters. In addition, the sequence needed to be adapted to parallel transmission to allow a whole-brain viable measurement. The integration of universal pulses has been carried out to proceed without further complex and time-consuming prior calibration.

2. Theory

By using fast repeated RF pulses interleaved with constant spoiling gradient area and direction, the (unbalanced) SSFP signal depends on many different parameters. On the one hand, for a fixed TE, the sequence parameters such as TR, flip angle and quadratic phase cycling, as well as gradient direction and area can be varied. On the other hand, under the Bloch-Torrey model assumption, valid for liquids under free diffusion, the signal depends on different physical parameters such as PD, T_1, T_2, and diffusion coefficient, as well as the intensity of the transmit B_1^+ field. QuICS (13–15) is based on the sequential and/or periodically interleaved acquisitions of several SSFP k-spaces with different contrasts obtained by varying RF spoiling, prescribed FA, and/or spoiling gradient area of the sequence. A fitting is then performed using the Bloch-Torrey equations providing a quantitative representation of the various contrasts. Based on an a priori range for tissue properties (expected SNR, B_1 inhomogeneity, T_1, T_2, diffusion coefficient), the sequence parameters can be optimized beforehand to reduce bias and increase precision of the physical parameters estimates.

2.1. SSFP signal model in the configuration states formalism

In SSFP, the FA is repeated with a fixed amplitude and RF spoiling is applied with a quadratic phase cycling scheme characterized by the phase increment Φ_{inc}. In this work, the spoiling gradient was applied along the readout direction in a gradient-echo sequence with a standard Cartesian k-space sampling.

The spoiling gradient area is characterized by the parameter N_{RO}, the number of 2π-dephasing over the readout direction. It is supposed that N_{RO} is an integer, such that, consistently with the so-called configuration-state formalism (27,28), both the longitudinal M_Z and transverse M_{XY} magnetization can be written as in (15). The two phase encoding directions were fully balanced. A measurement necessarily corresponds to a single order of the transverse magnetization. The order can be selected by changing the gradients applied before and after the readout, respectively (see DESS or TESS). Here, only the zeroth-order at the steady-state was measured, and thus needs to be simulated with a given signal model.

The configuration state formalism can be used to simulate the effects of the above-described SSFP sequence in a compact way for an efficient fitting. It was chosen here to consider the Bloch-Torrey equations in free space (unrestricted). Under these assumptions, the effects of T_1 and T_2 relaxation times, diffusion, gradient spoiling, and the application of an RF pulse can all be expressed as linear operators. T_1 and T_2 relaxation times induce an attenuation of the vector's elements (29); recovery is also accounted for by adding a constant to longitudinal magnetization; the free Gaussian diffusion can be modeled as a multiplication with a Gaussian kernel(30,31); a gradient induces an index shift; and RF acts as a transfer between longitudinal and transverse components, assuming here an instantaneous action. After a sufficiently large number of excitations, a steady-state is reached. The only information needed being the steady-state, the calculation can be efficiently solved using the fast algorithm described elsewhere (13,15) to simulate the signal.

2.2. Multiparametric quantification

We consider here multiple (N) acquired SSFP contrasts from which quantitative extraction of model parameters is aimed. In the following, the different contrast measurements will be noted S_c where c denotes the measurement index, from 1 to N. The corresponding model calculated from the Bloch-Torrey equations simulated for a set of varying sequence parameters $\{FA_{target}, \Phi_{inc}\}_c$, with fixed sequence parameters {TR, TE, N_{RO}} will be noted m_c. FA_{target} refers to the target flip angle and Φ_{inc} is the RF spoiling increment. The algorithm was implemented in Matlab (The Mathworks, Natick, USA) on complex images to 1) remove unwanted phase

drifts from the DICOM files, 2) to extract the quantitative parameters voxel-wise and 3) to correct for receive-sensitivity bias to retrieve proton density images from M_0.

2.2.1. Unwanted phase removal

First, global phase drifts were removed, assuming a linear temporal evolution between the first and last volumes, acquired in the same conditions. A phase map was estimated using the complex sum of first and last volumes with no RF cycling ($\Phi_{inc} = 0°$ and 360°). Due to off-resonance effects during scanning, the phase of this sum is of the form:

$$\varphi_{\mathrm{TE}} = \gamma \Delta B_0 TE + \varphi_1 \qquad \text{Eq. 1}$$

where $\gamma \Delta B_0 TE$ accounts for the ΔB_0 -induced phase accumulation, and φ_1 accounts for the RF phase (combining transmission and reception). The multiple measurements S_c were phase-corrected using this estimation, leaving phase effects only linked to the SSFP signal, free of the above-mentioned factors, particularly for B_0 inhomogeneities.

2.2.2. Least-squares problem formulation

To perform the quantitative extraction of the different NMR parameters, the inverse problem is expressed as the following non-linear least-squares minimization between the corrected complex measurements and the model:

$$\min_{M_0, T_1, T_2, FA} \sum_{c=1}^{N} \| S_C - M_0 \times m_c(T_1, T_2, FA) \|^2 \qquad \text{Eq. 2}$$

In the present demonstration in vivo at 7T, instead of neglecting diffusion effects, it was chosen to account for it by setting it to a value of $D=0.8.10^{-3}$ $mm^2.s^{-1}$, i.e. in the order of reported data for white matter (WM) and grey matter (GM)(32). An initialization step was performed using a coarse dictionary comparison, followed by the application of a Gauss-Newton algorithm based on the Jacobian matrix, expressed with real and imaginary parts, defined in Eq. 3.

$$\mathrm{J} = \begin{pmatrix} real(m_c) & real\left(\frac{\partial m_c}{\partial T_1}\right) & real\left(\frac{\partial m_c}{\partial T_2}\right) & real\left(\frac{\partial m_c}{\partial FA}\right) \\ imag(m_c) & imag\left(\frac{\partial m_c}{\partial T_1}\right) & imag\left(\frac{\partial m_c}{\partial T_2}\right) & imag\left(\frac{\partial m_c}{\partial FA}\right) \end{pmatrix} \qquad \text{Eq. 3}$$

Performed voxel-wise, this iterative and non-linear method allowed the retrieval of multiple quantitative maps of M_0, T_1, T_2 and FA.

2.2.3. Proton density retrieval

To retrieve a quantitative proton density map from the estimated M_0, the sensitivity profile of the coil was assessed as proposed in (33) using 3rd order three-dimensional polynomial and removed from the M_0 maps.

2.3. Protocol optimization

To optimize the acquisition time for clinical applications, the number of contrasts to acquire was limited to the most informative sequence parameters $\{FA_{target}, \Phi_{inc}\}_c$, using Fisher Information theory. Let us denote by θ_i, i=[1,2,3,4] the parameters to be estimated (M_0, FA, T_1, T_2), and m_c the different signals obtained from the model. These signals depend on θ_i, on the noise (zero mean Gaussian with a variance σ^2) but also on the sequence and physical parameters. To optimize the acquisition parameters, it is meaningful to maximize the Fisher Information Matrix (FIM), that can be defined as(13):

$$FIM = \left(\frac{|M_0|}{\sigma}\right)^2 J^H J \qquad \text{Eq. 4}$$

Where σ is the standard deviation of the noise and J is the Jacobian matrix, defined in Eq. 3.

The FIM measures the information carried by the observation m_c on the parameters θ_i. This FIM is closely linked to the Cramér-Rao lower bound (CRLB), defined in Eq. 5, which gives a lower bound for the standard deviation σ_{θ_i} in the estimation of the parameter θ_i.

$$\sigma_{\theta_i} \geq CRLB_i = \sqrt{(FIM^{-1})_{ii}} \qquad \text{Eq. 5}$$

To restrict the acquisition protocol to the most informative contrasts, the cost function to minimize, CF, was defined as the sum of the normalized CRLB over the number of parameters to estimate, $N_{par} = 4$ (Eq. 6).

$$CF = \sum_{i=1}^{N_{par}} \frac{\sigma_{\theta_i}^2}{\theta_i^2} \qquad \text{Eq. 6}$$

The most adequate acquisition parameters to optimize the assessment of the targeted relaxation times (T_1 ranging from 0.3 to 3.5s and T_2 from 10 to 200ms), with an effective flip angle ranging from 0.2 to twice the targeted FA, were determined using a Self-Organizing Migration Algorithm (SOMA) with 100 stochastic migrations (34). The considered range for phase increments varied from 0 to 360°. The assessment of diffusion would require an N_{RO}>>1 to have enough diffusion sensitivity in the sequence. However, to extract only relaxation times, low spoiling conditions can be sufficient. N_{RO} was experimentally fixed to 4, for all RF spoiling

increments, as a compromise between a reduction of the influence of through-voxel B0 gradients and mitigation of flow- and motion-induced phase errors, while keeping a good accuracy in the quantitative extraction (see Supporting Information Figure S1 and Figure S2). Such strategy also prevents through-voxel B_0 gradients in the tissues that could affect the spoiling efficiency, and therefore the extracted parameters (35). To reduce SAR as much as possible, the maximum FA allowed for the series was restricted to 30°. For this number of parameters to estimate (M_0, FA, T_1, T_2), the best compromise between acquisition time and quantitative parameters' accuracy was the acquisition of 11 contrasts (see Supporting Information Figure S3). The resulting acquisition parameters are shown in Table 1.

Contrast #	**1**	**2**	**3**	**4**	**5**	**6**	**7**	**8**	**9**	**10**	**11**
FA_{target} (°)	30	8	29	3	29	13	28	8	29	17	30
RF incr. (°)	0	358	9	1	77	359	1	2	1	358	360

Table 1 : Acquisition setup resulting from the optimization process for 11 contrasts and a 1.0x1.0x3.0mm^3 acquisition using a fixed N_{RO}=4.

3. Methods

3.1. In-silico evaluation

To determine the sensitivity of such QuICS protocol to the transmit inhomogeneity encountered at UHF, we analyzed by means of Monte-Carlo simulations how the parameters estimations vary with the effective FA. The acquisition setup presented above was simulated, varying the FA from 0 to twice the targeted FA by 1° steps, using 10,000 samples per FA. The ability of the quantification algorithm to reliably assess our targeted parameters, here WM (T_1=1.3s, T_2=55ms), GM (T_1=2.0s, T_2=50ms) and voxels including CSF (T_1=3000ms, T_2=150ms)(36), is reported in Figure 1. These results show a relative immunity to the effective FA down to 50% of the targeted FA. Below this value, the extracted parameters will present a bias, but also a larger variance, resulting in a reduced SNR in the quantitative maps. A graphic illustration is presented in

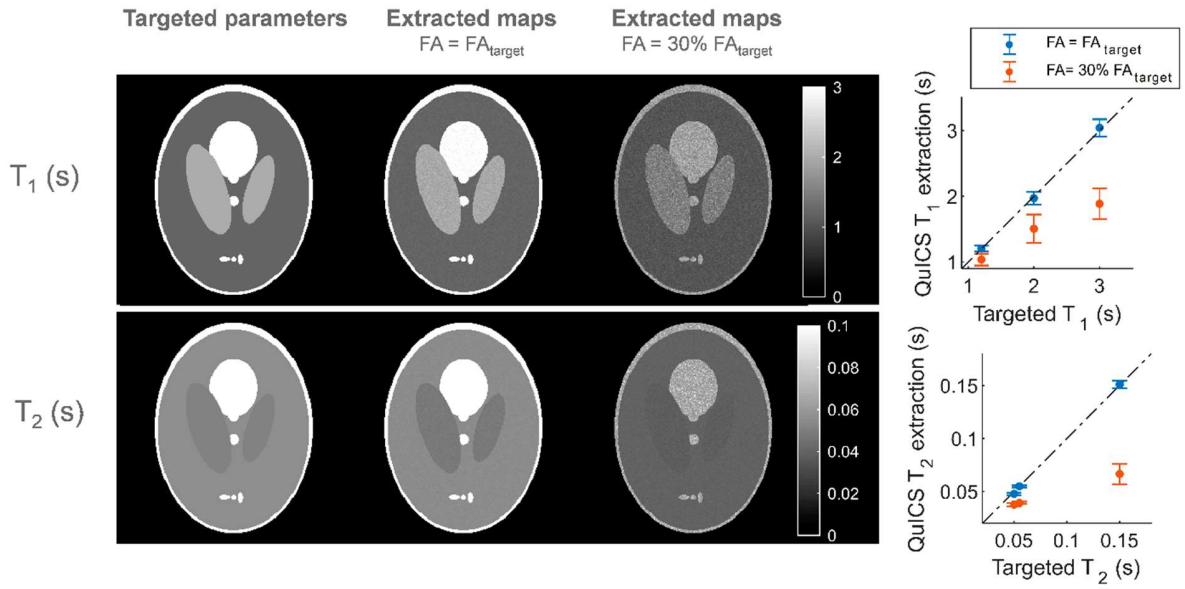

Figure 2, where simulations were performed with the targeted FA, and with a FA of 30% of the target for the same input M_0 (reflecting the SNR level). As can be seen, the SNR of the quantitative maps is reduced, in addition to a bias in the quantitative maps. In the human brain at 7T, such loss of B_1^+ is typically encountered, particularly in the cerebellum and temporal lobes.

3.2. MRI acquisitions

Measurements were performed on a Magnetom 7T scanner (Siemens Healthineers, Erlangen, Germany) equipped with the Nova 8Tx-32Rx head coil and an SC72 whole body gradient insert (max gradient amplitude 100mT/m and max slew rate 200T/m/s). The study was conducted with the approval of the Institutional Review Board (IRB) and all volunteers gave written informed consent.

3.2.1. Phantom acquisitions

The reliability of the derived protocol was tested on a small phantom deprived of strong B_1^+ inhomogeneity. The phantom was composed of four 50mL Falcon tubes containing 1% of agar and gadolinium-based contrast agent (Gadoterate meglumine, Dotarem, Guerbet, Aulnay-sous-bois, France) at various concentrations of 0, 1.25, 2.5 and 5mM. Theoretical T_1 and T_2 of the phantoms were retrieved using Eq. 7:

$$\frac{1}{T_i} = \frac{1}{T_{i,0}} + r_i C \qquad i = 1,2 \qquad \text{Eq. 7}$$

Where $T_{i,0}$ is the relaxation time in absence of contrast agent, r_i is the relaxivity of the contrast agent and C its concentration. We used r_1=4,4 $mM^{-1}.s^{-1}$ and r_2=4,8 $mM^{-1}.s^{-1}$ measured at 7T in our laboratory in the same conditions (37).

The QuICS protocol described above was acquired with TR/TE=11ms/3.3ms, bandwidth=650Hz/px. The image resolution was 1.0x1.0x3.0mm^3 in a 256x160x168mm^3 field-of-view, and a GRAPPA acceleration factor of 3 was applied, leading to a total acquisition time of 8min18s.

Actual T_1 and T_2 of the phantoms were assessed using standard established methods that are feasible in vivo. In the following, they will be referred to as the "reference" methods. T_1 was obtained using the Variable Flip Angle technique (VFA or DESPOT1), with FAs of 5 and 20°, TR/TE=14/3ms, at a 1.0x1.0x3.0mm^3 resolution obtained in 3min16s. To correct for incomplete spoiling and B_1^+ inhomogeneities as proposed in (38), an Actual Flip angle Imaging sequence was used (39,40), with a resolution of 4mm isotropic, TE=3.06ms, BW=150Hz/px, FA=60°, TR_1+TR_2=130ms and TR_2/TR_1 = 5, leading to an acquisition time of 5min26s. Reference T_2 map was measured using multiple segmented single-echo spin-echo sequences, with TE=10/30/50ms, TR=8s, resolution of 2.0x2.0x3.0mm^3, and EPI factor of 3. The total scan time for B_1 mapping, VFA and multi-spin-echo was of 26 minutes.

3.2.2. In vivo acquisitions

MRI acquisitions were performed on six healthy volunteers (3 females/3 males, age 22.6±2.7 years-old). Acquisitions consisted of a 3D Cartesian unbalanced SSFP, using non-selective 500µs rectangular pulse in circularly-polarized mode (CP-mode), but also using a scalable non-selective k_T-point Universal Pulse (26) to obtain a homogeneous FA distribution. The universal k_T-point solution was designed offline on a database of 20 B_1^+ and B_0 field maps from a prior study, to be robust to inter-subject variability(41). The duration of the UP was set to 3.25ms in order to yield the same input total power of 1.8W for the CP-mode and the UP acquisition. According to the electromagnetic simulations provided by the coil manufacturer, our in-house calibration/validation procedure and a 2.3 safety factor (42) on the most SAR-demanding volume, the UP lead to a global SAR and a maximum local SAR of 0.245W/kg and 1.330W/kg respectively, versus 0.275W/kg and 2.25W/kg for the CP pulse. Measurements were performed under Siemens Healthineers "Protected mode" which imposes that the average input power per transmitting channel measured at the coil's plugs does not exceed 1.5W and that the sum over the channels (c) of the average input power ($\bar{P}$) does not exceed 8W:

$$\bar{P}_c < 1.5W \qquad \text{Eq. 8}$$

$$\sum_{c}^{8} \overline{P_c} < 8W \qquad \text{Eq. 9}$$

QuICS scanning parameters were TR/TE=11ms/3.3ms, bandwidth=650Hz/px. Native transversal orientation was chosen for 3D 256x160x168mm^3 field-of-view (FOV) with a 1.0x1.0x3.0mm^3 spatial resolution to ensure maximal image quality in the radiologists' preferred reading plane. Therefore, to avoid aliasing artefacts, an oversampling of 100% was added in the slice direction (twice the FOV along this axis effectively sampled). A GRAPPA acceleration factor of 3 was applied along the phase encoding direction, leading to a total acquisition time of 16min36s.

Reference PD, T_1 and T_2 maps were also measured in vivo using VFA and multi-spin-echo acquisitions described above for phantoms acquisitions in a total time of 26 minutes.

3.2.3. Brain segmentations

A segmentation of the acquired contrasts with UP was performed using the Advanced Normalization Tools (ANTS) Cortical Thickness pipeline (43) with Open Access Series of Imaging Studies (OASIS)(44) as templates and priors. For the six scanned subjects, GM and WM masks were extracted. Mean values of PD, T_1 and T_2 were then estimated for both regions in QuICS volumes and corresponding references' slices acquisitions.

3.3. Synthetic imaging

Synthetic contrast-weighted images could be retrieved from the quantitative data, using equations describing the signal intensity as a function of acquisition parameters and measured NMR parameters. First, a T_2-weighted contrast from Fluid Attenuation Inversion Recovery (FLAIR) technique was computed using Eq. 10 with TR=6s, TE=120ms and inversion time TI of 2.2s(45).

$$S_{FLAIR} = M_0 \left(1 - 2\,\mathrm{e}^{-\frac{TI}{T_1}} + e^{-\frac{TR}{T_1}}\right) e^{-\frac{TE}{T_2}} \qquad \text{Eq. 10}$$

A T_2-weighted contrast was synthesized from spin-echo with TR=6s and TE=90ms. Finally, GRE contrast was estimated using a homogeneous targeted FA of 20°, TR=30ms and TE=2ms following Eq. 11.

$$S_{GRE} = M_0 \left(\frac{1 - e^{-\frac{TR}{T_1}}}{1 - e^{-\frac{TR}{T_1}}\cos(FA)}\right) \sin(FA)\, e^{-\frac{TE}{T_2}} \qquad \text{Eq. 11}$$

4. Results

Quantitative results obtained on a phantom containing samples with different relaxation times are displayed in Figure 3. Exemplary in vivo contrasts obtained from optimized sets of Table 1 are shown in Figure 4, demonstrating the complex modulation of the signal.

Figure 5 depicts masks of the brain where a threshold of 50% of the targeted FA was considered. The area where FA is lower than 50% of the target, in red, was reduced by 54% on average over the six scanned subjects when applying parallel transmission UPs. The corresponding parametric maps, for which an example is displayed for one subject in Figure 6, demonstrate a drop in cerebellum and temporal lobes for all the quantitative values in CP-mode, as expected from the Monte-Carlo simulations presented above. After applying UP, the FA map is much more homogeneous, and quantitative results are acceptable over the whole brain. No quantitative analysis could be performed for FA comparison with UP due to limited acquisition time, but Supporting Information Figure S4 presents qualitative comparison of QuICS and AFI retrieved flip angle maps in CP-mode.

Figure 7 presents visual comparison between reference methods and QuICS' resampled results for the same slice. 2D histograms and corresponding regression demonstrate a slope of 0.99 and 0.98 for T_1 and T_2 respectively. A reproducible overestimation bias of 324.1ms is observed in T_1. Mean PD, T_1 and T_2 values obtained over the six volunteers after segmenting brain quantitative maps obtained with QuICS and reference values are reported in Table 2. Individual quantitative results from QuICS and reference methods are also presented in Supporting Information Table S1. Overall, presented results are in the same range and in agreement with literature reported values (36,46) and demonstrate a good reproducibility. It is important to note that GM results are impaired by partial volume with CSF. Synthetic images retrieved from retrieved quantitative maps using UPs are shown in Figure 8.

	Mean PD ± s.d (p.u)		**Mean T_1 ± s.d (ms)**		**Mean T_2 ± s.d (ms)**	
	QuICS	**VFA**	**QuICS**	**VFA**	**QuICS**	**SE**
White matter	0.59±0.01	0.58±0.01	1698.1±65.3	1400.4±50.9	33.7±0.7	38.0±4.9
Grey matter	0.68±0.01	0.67±0.02	2577.0±76.4	2167.2±165.2	49.2±3.8	34.3±5.3

Table 2: Mean PD, T_1 and T_2 in white and gray matter over the 6 scanned subjects, obtained with QuICS acquisition using Universal Pulses over the whole brain and reference methods in the available slices. CSF results are not displayed: the coarse slice thickness lead to unreliable segmentation for this region. Pulsatile motion also leads to corrupted signals in the different contrasts in this region, and therefore to unreliable quantification for such long T_1 and T_2. GM results are also impaired by this resolution and suffer from partial-volume with CSF.

5. Discussion

Quantification techniques using UHF could lead to a greater characterization of disorders (2). In this work, we have described an acquisition protocol at 7T which combines the QuICS and the pTx UP approaches. We have demonstrated that their association allows robust assessment of 3D quantitative maps of PD, FA, T_1, and T_2 at a resolution of 1.0x1.0x3.0mm^3 in 16min36s.

We have shown that it is possible to obtain a sequence parameter set $\{FA_{target}, \Phi_{inc}\}_c$ for eleven contrasts that optimized the estimation of targeted physical parameters (M_0, FA, T_1, T_2) for different tissues types under the constraint of a maximum FA (30° here). The obtained parameter set is not unique to fulfil the optimization criterion. Here, the optimization process led to some volume acquisitions with large flip angles (close to 30°) and different phase increments, and others with lower flip angles and phase increments close to 0° or equivalently 360°. This suggests that both flip angle magnitude and phase are modulating the steady-state signal in an informative way. Further work would be needed to understand the influence of flip angle and phase increment patterns on extracted parameters' accuracy (34). Here, the sum of the relative errors was chosen as a cost function, in order to weight each parameter identically. However, it would also be possible to apply the same optimization protocol with non-unity parameter weights, to emphasize improved precision for some of the parameters at the expense of the others.

Monte-Carlo simulations of the performance of QuICS to estimate the parameters have confirmed the sensitivity of the method to the actual FA. As a simple rule, if the latter is lower than 50% of the targeted FA, the bias in the parameter quantification becomes significant, and the SNR of the quantitative maps is impaired, as shown in

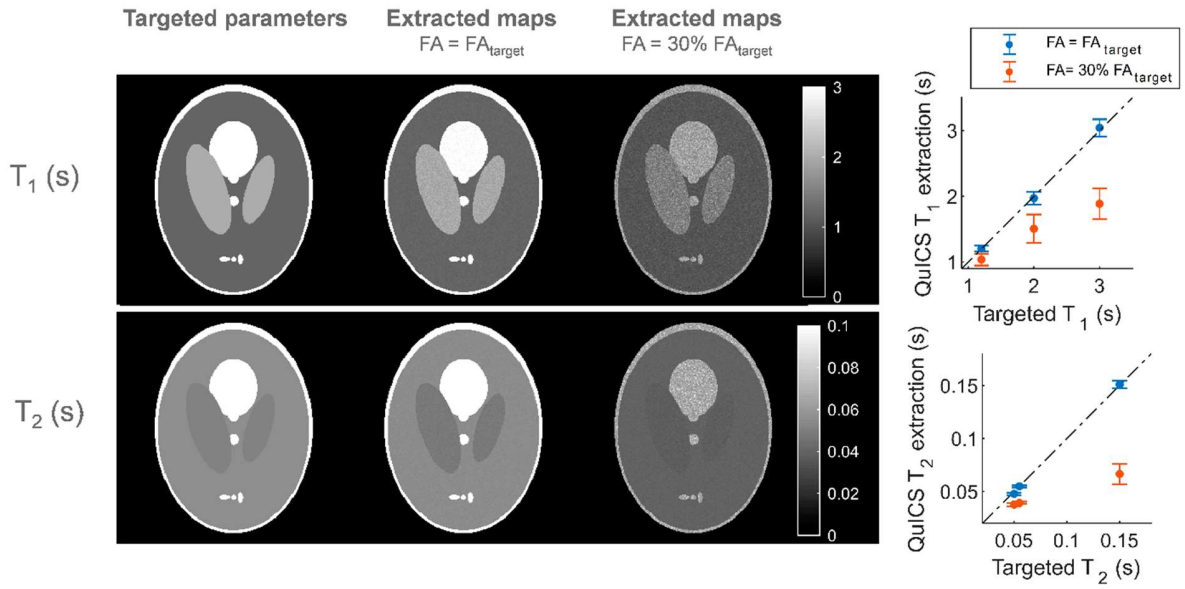

Figure 2. Indeed, in such scenario, the spectrum of attained FAs during the protocol is too restricted, resulting in a lowered sensitivity in the extraction of NMR parameters. With the 8Tx-32Rx Nova head coil driven in quadrature, we have also verified that a significant portion of the brain falls in regions of low transmit efficiency where the actual to targeted FA ratio can be below this threshold.

The proposed QuICS protocol was first applied on small (with the purpose to reduce the effect of B_1^+ variations) phantoms implementing various relaxation times using the CP-mode of the RF coil. Estimated relaxivities were in agreement with Monte-Carlo simulations and reference methods, validating the presented model and the optimization procedure for the acquisition parameters.

To translate this proof-of-concept to in vivo acquisitions where B_1^+ inhomogeneity increases dramatically, parallel transmission UPs were applied to keep clinical applications possible. Figure 5 confirms the ability of the UPs to efficiently mitigate the B_1^+ field inhomogeneity on a SSFP sequence with various FA and RF spoiling increments. The 3D results shown in Figure 6 demonstrate a robust extraction provided that the effective FA is greater than half of the targeted FA, confirming the Monte-Carlo simulations presented in

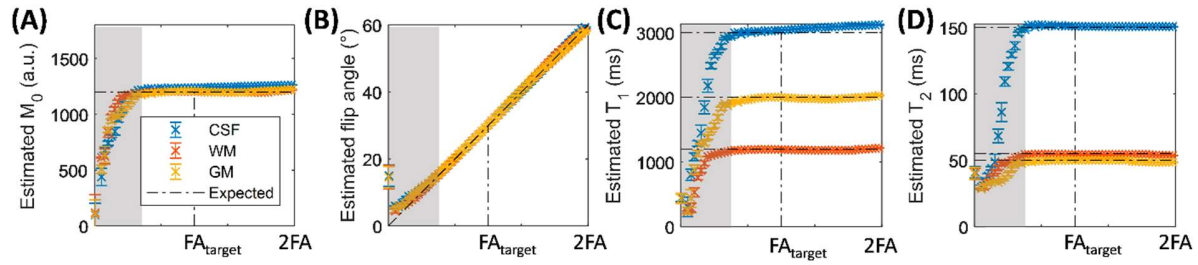

Figure **1**. The use of UPs improves the robustness of QuICS for in vivo relaxometry at 7 Tesla thanks to a globally restored FA over the whole brain.

Since the FA and RF increment schedule was precisely chosen to maximize the Fisher information, the proposed approach reduces biases and noise in the extraction, while reducing the acquisition time. Here, when considering the acquisition of both T_1 and T_2, reference methods failed to achieve the same resolution and FOV coverage, for a longer acquisition time.

When comparing the assessed parameters over the whole brain with reference methods (Figure 7 and Table 2), T_1 values are higher than those obtained with VFA, as illustrated in Figure 7. Magnetization transfer effects might play a role in that effect (47–49). Moreover, relaxation effects during the pulse were not considered in the quantitative extraction of parameters. This might affect the retrieved signal, as shown in literature (50), and will be the subject of future work. It is also important to note that the "reference methods" chosen here to perform comparisons are usually well accepted at lower field strengths, but their capability to recover reliable and unbiased relaxation rates at UHF still needs to be demonstrated (51,52). When looking into more details at the GM and WM relaxometric values obtained from the brain segmentations of the quantitative maps in Table 2, QuICS retrieves consistent results with values previously reported in literature at this field strength (36). The presented GM estimations demonstrate an overestimation for both T_1 and T_2 due to a slice thickness of 3mm, resulting in partial volume from the CSF in the GM mask.

Nevertheless, these observations do not invalidate the multiparametric approach studied here. Dictionary-based methods come with a long post-processing step at UHF (22). Here, the extraction of quantitative maps directly from DICOM images was achieved in approximately 26 minutes on a laptop (2.6GHz Intel i7-5600 processor). This process could easily be improved using parallel computing, opening perspectives for a clinical workflow compatibility.

Future clinical use of quantitative MRI could be facilitated by the application of synthetic MRI. Visually, the retrieved contrasts were in agreement with the usual tissue contrasts obtained with conventional acquisitions. Here, simplified models were used to create such contrasts, excluding MT effects or relaxation during RF pulse. From the quantitative T_1, T_2 and PD maps, virtually any contrast-weighted image could be generated from the Bloch equations. Such simultaneous multi-parametric mapping method could therefore potentially replace the acquisition of multiple conventional images and save valuable scanner time (3).

For a better clinical applicability, the different contrasts (shown in Figure 4) obtained in a single acquisition could be split to reduce the scanning time of one sequence for patients. More importantly, the total acquisition time could easily be shortened by diminishing the acquisition oversampling and changing the acquisition orientation to sagittal. The same protocol could also be adapted by replacing the non-selective UP excitations by Universal slab-selective multi-spoke excitations, allowing a drastic gain of time (41). Another strategy to accelerate acquisition time would be to use non-Cartesian k-space trajectories (53). On the one hand, the resulting time reduction could be used either to speed up this protocol or to retrieve an additional ADC map(15). Indeed, one-dimensional ADC maps were recovered in vitro, but were discarded in this study as they become of limited information in anisotropic media such as human brain. A proper trace ADC estimation would require multiple spoiling directions, and more contrasts would therefore be needed. On the other hand, these modifications can also impair the SNR, leading to reduced parameter precision. As it is still possible to increase the maximum FA and the NRO values, this could also be evaluated as means to gain precision. In all cases, new sequence protocol optimization will be required to account for these new situations.

.

6. Conclusion

This work is the first application of QuICS at UHF using parallel transmission and calibration-free Universal Pulses. The method showed its ability to accurately measure PD, FA and relaxation times over the whole brain. Measured parameters were in good agreement with previously reported values in the literature and effective reference measurements. The robustness of the approach was validated over six healthy adults. Such quantitative method is of interest for clinical research studies at UHF where the fast and robust assessment of several NMR physical parameters could represent a real added-value in the diagnosis process, as correlations between different tissue properties might lead to improve patient outcome (3,4).

Figures

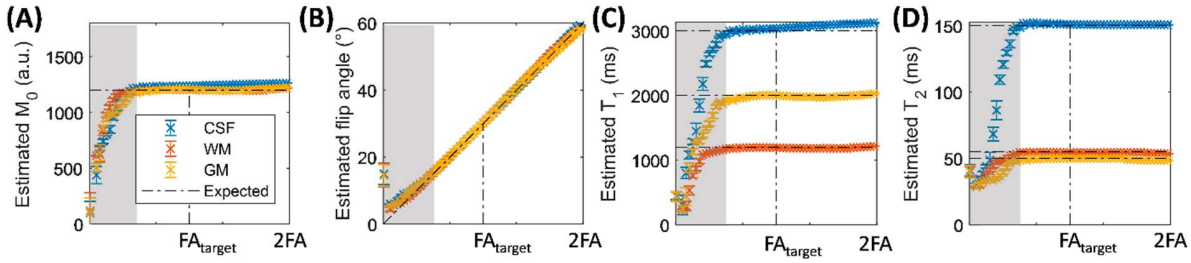

Figure 1 : Monte-Carlo simulations of M_0(a), FA(b), T_1(c) and T_2(d) estimations as a function of effective FA, in order to account for its variations at UHF, considering ADC fixed to $0.8.10^{-3}$ $mm^2.s^{-1}$, for voxels including cerebral spinal fluid (CSF) in blue (T_1=3.0s, T_2=150ms), white matter in orange (T_1=1.2s, T_2=55ms) and grey matter (T_1=2.0s and T_2=50ms). This figure illustrates that for a FA lower than $FA_{target}/2$ (shaded area), the quantitative extraction process fails to obtain reliable values of M_0, FA, T_1 and T_2. The strong biases encountered on quantitative extractions while deviating from targeted FA justifies the need of a pTx dynamic shim strategy.

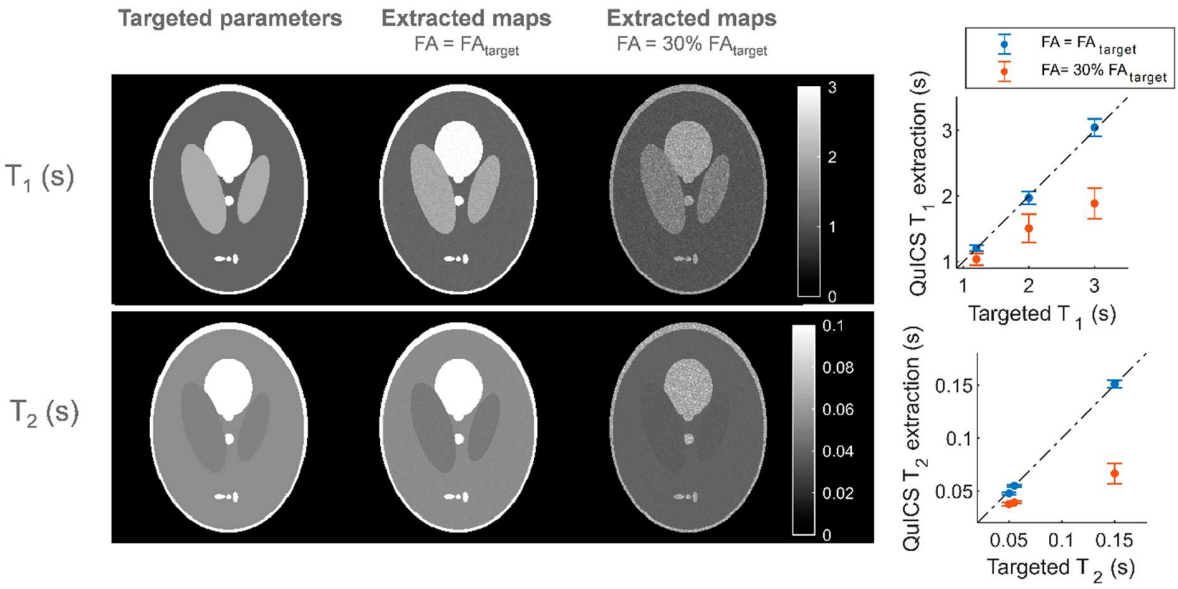

Figure 2 : QuICS simulations were performed on a 256x256 Shepp-Logan phantom divided in 3 ROIs with physiological values of white matter (T_1=1.3s, T_2=55ms), gray matter (T_1=2.0s, T_2=50ms) and voxels including CSF (T_1=3000ms, T_2=150ms). Simulations were done with the targeted flip angle, and with a flip angle of 30% of the target for the same input SNR. The mean value in each ROI is reported with its standard value. As can be seen, if the flip angle is too low, the quantitative maps exhibit a bias as well as a lower SNR.

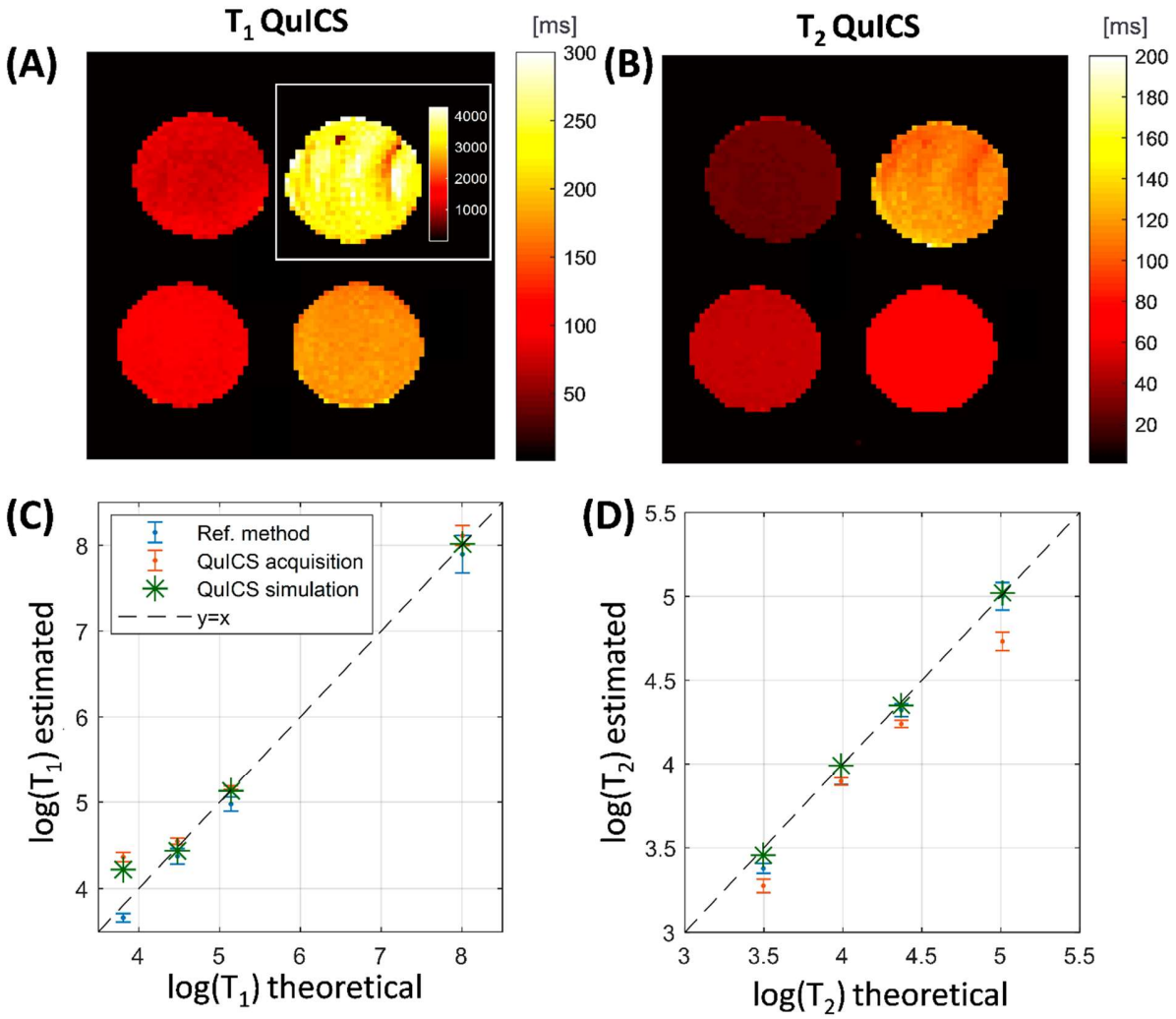

Figure 3 : Central slice of the QuICS extraction at 7 Tesla on a phantom with four tubes of varying gadolinium concentrations for (a)T_1 and (b)T_2. The comparison of the results obtained between QuICS and a reference method (VFA or multi-spin Echo respectively) in a central circular ROI of diameter 8mm are shown in c) and d). Theoretical relaxation times were retrieved from Eq. 7. The logarithms of relaxation times are plotted for a better visualization.

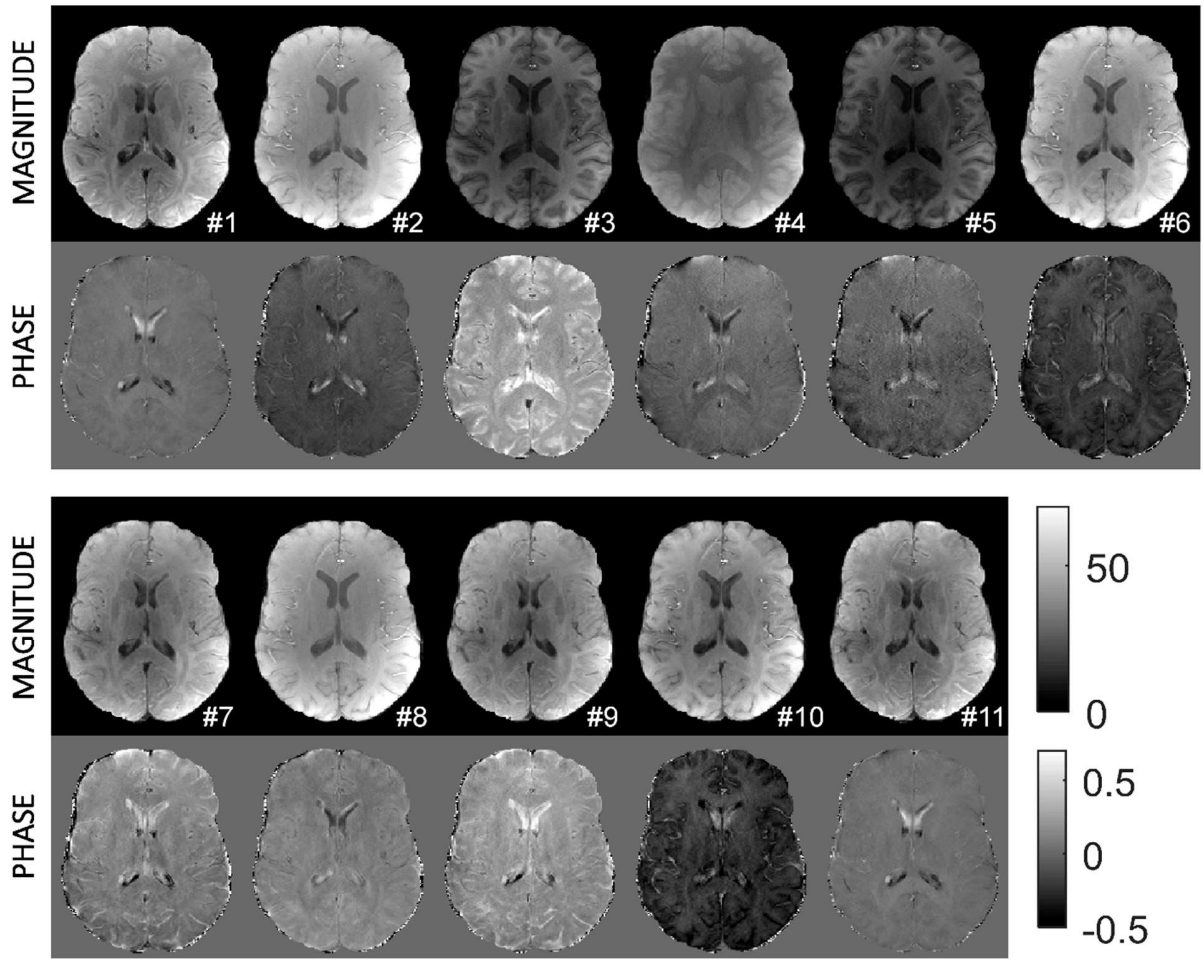

Figure 4 : Retrieved magnitudes and phases for the 11 contrasts obtained in vivo at 7T when acquiring the setup from Table 1 at a 1.0x1.0x3.0mm^3 resolution (subject #4).

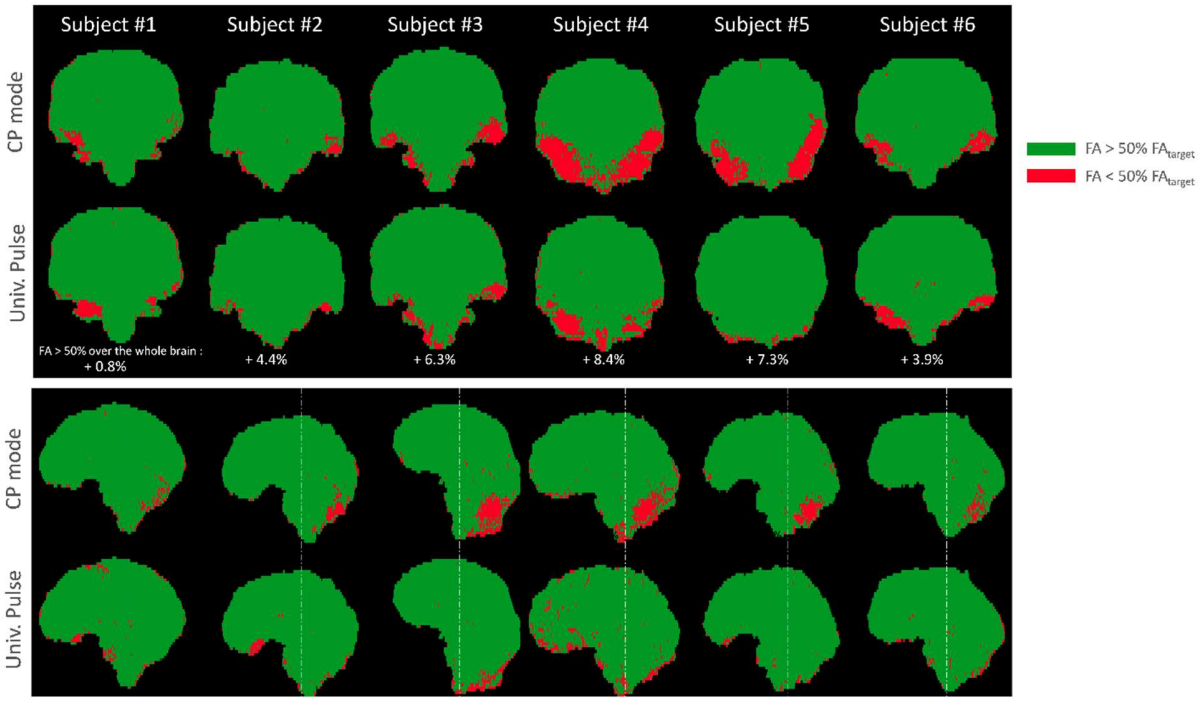

Figure 5: Masks of the 6 scanned subjects showing the areas where the flip angle was higher than 50% of the targeted FA (in green, defined as the limit below which QuiCS leads to biased estimations), comparing the CP mode and Universal Pulse. The displayed coronal slices are at the position indicated by white dotted lines, and central sagittal views are shown. The use of UP allowed the green region to grow systematically over the whole volume, as indicated by the figures for each subject.

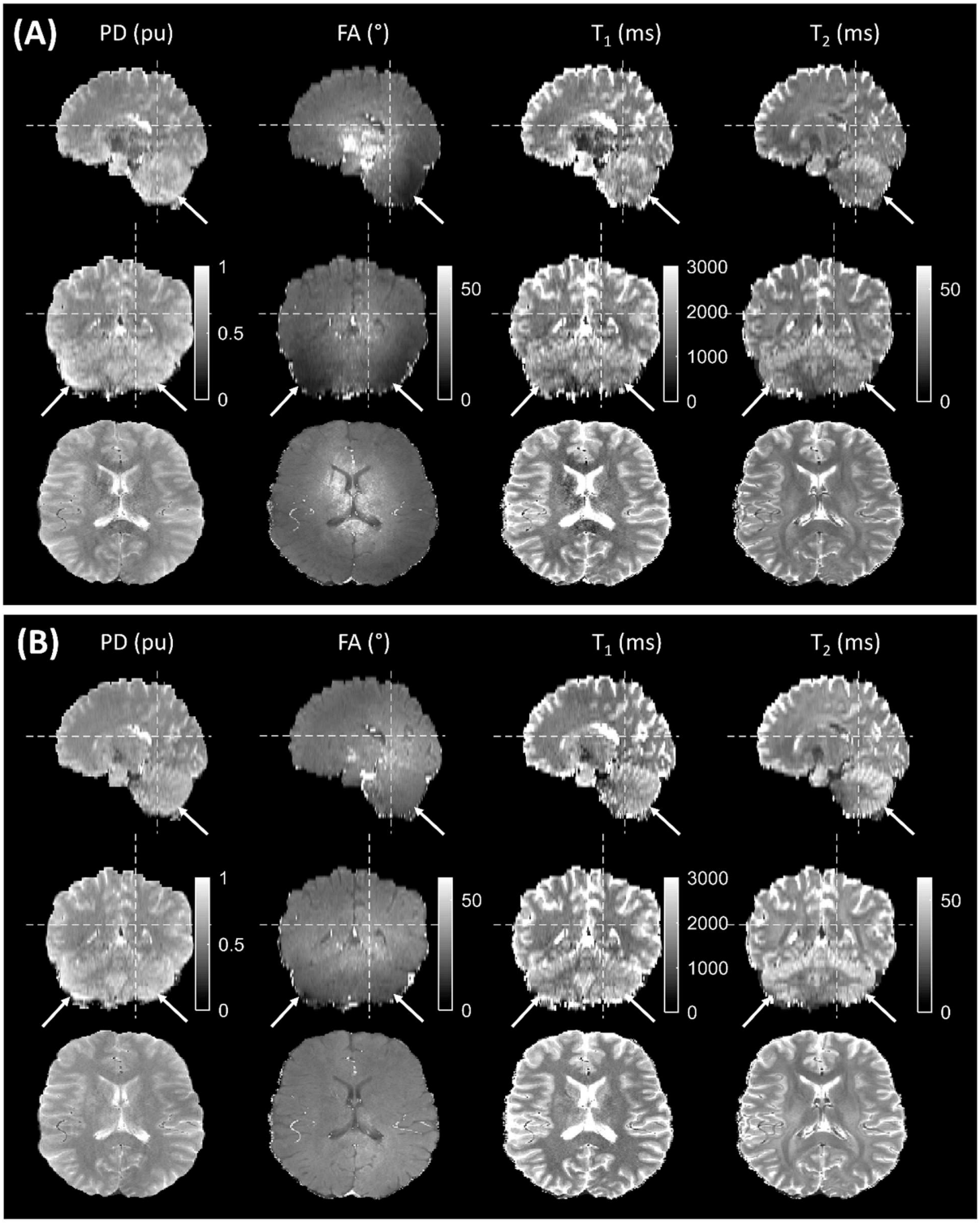

Figure 6: 7T 3D QuICS (1x1x3mm^3) quantitative extraction for PD, flip angle, T_1 and T_2 maps using (A) rectangular pulse, (B) Universal Pulse excitation on subject #2. Displayed slices are depicted in the 3

different orientations by white dotted lines. In (Q), QuICS fails to estimate properly the quantitative parameters in the cerebellum and temporal lobes, due to a high FA inhomogeneity, as highlighted by arrows. In (B), the flip angle distribution is much more homogeneous, and the QuICS extraction was successful over the whole brain, particularly in areas where the CP-mode implementation failed (a).

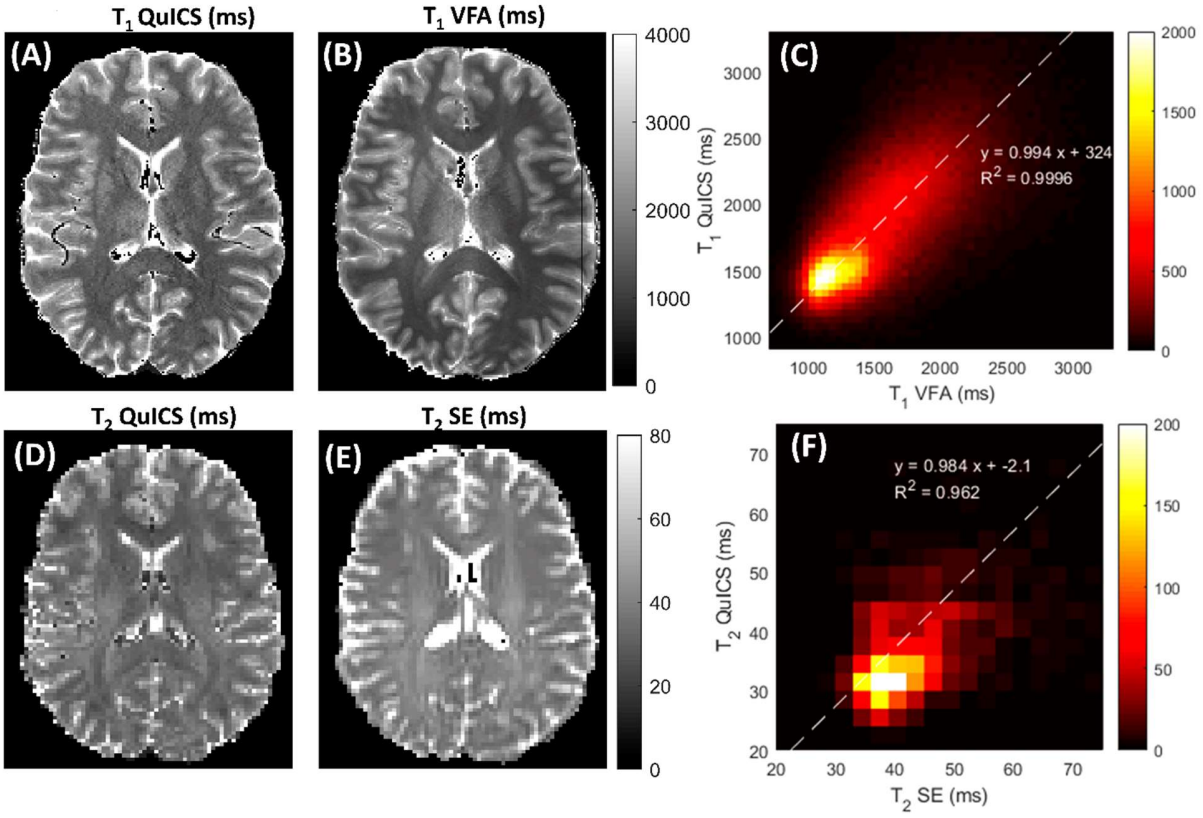

Figure 7: Central T_1 maps obtained using QuICS (A) and VFA(B) methods are presented. Corresponding 2D histogram of the reference acquisition compared to the extracted QuICS parameters with UP for subject #2 over the whole brain is presented in (C). The same slice is presented for T_2 maps retrieved with QuICS resampled to a 2-mm in-plane resolution (D) and multiple single-spin-echo (E). (D) was undersampled to match (E) resolution. Corresponding 2D histogram of the slice is presented in (F). Results demonstrate an overestimation of 324.1ms for T_1, and underestimation of 2.1ms for T_2, with an overall very good correlation of 0.994 and 0.984 between QuICS and reference methods.

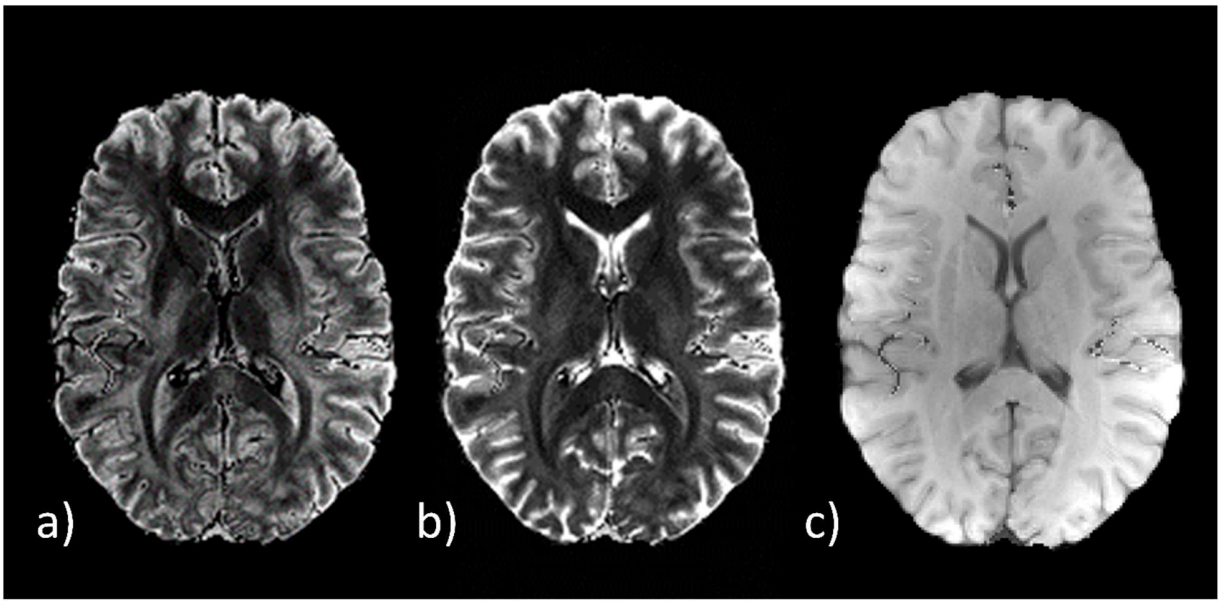

Figure 8: Synthetic contrasts retrieved from the quantitative results obtained from QuICS for subject #2. Weighted contrast based on FLAIR signal with TR=6s, TE=120ms, TI=2.2s (a), T_2-weighted contrast from a Spin-Echo signal with TR=6s and TE=90ms (b), and Gradient-Echo contrast with FA=20°, TR=30ms and TE=2ms (c) are presented.

Acknowledgments

This work received financial support from the French program 'Investissement d'Avenir' run by the 'Agence Nationale pour la Recherche', grant 'Infrastructure d'avenir en Biologie Santé – ANR-11-INBS-0006', from the ERPT equipment program of the Leducq Foundation, and from the European Union Horizon 2020 Research and Innovation program under Grant Agreement No. 736937.

References

1. Voelker MN, Kraff O, Brenner D, et al. The traveling heads: multicenter brain imaging at 7 Tesla. Magn. Reson. Mater. Phys. Biol. Med. 2016;29:399–415 doi: 10.1007/s10334-016-0541-8.

2. Cheng H-LM, Stikov N, Ghugre NR, Wright GA. Practical medical applications of quantitative MR relaxometry. J. Magn. Reson. Imaging 2012;36:805–824 doi: 10.1002/jmri.23718.

3. Warntjes J, Leinhard OD, West J, Lundberg P. Rapid magnetic resonance quantification on the brain: Optimization for clinical usage. Magn. Reson. Med. 2008;60:320–329 doi: 10.1002/mrm.21635.

4. Yu AC, Badve C, Ponsky LE, et al. Development of a Combined MR Fingerprinting and Diffusion Examination for Prostate Cancer. Radiology 2017;283:729–738 doi: 10.1148/radiol.2017161599.

5. Foucher JR, Mainberger O, Lamy J, et al. Multi-parametric quantitative MRI reveals three different white matter subtypes. PLOS ONE 2018;13:e0196297 doi: 10.1371/journal.pone.0196297.

6. Warntjes J, Dahlqvist O, Lundberg P. Novel method for rapid, simultaneous T1, T*2, and proton density quantification. Magn. Reson. Med. 2007;57:528–537 doi: 10.1002/mrm.21165.

7. Schmitt P, Griswold MA, Jakob PM, et al. Inversion recovery TrueFISP: Quantification of T1, T2, and spin density. Magn. Reson. Med. 2004;51:661–667 doi: 10.1002/mrm.20058.

8. Ma D, Gulani V, Seiberlich N, et al. Magnetic resonance fingerprinting. Nature 2013;495:187–192 doi: 10.1038/nature11971.

9. Jiang Y, Ma D, Seiberlich N, Gulani V, Griswold MA. MR fingerprinting using fast imaging with steady state precession (FISP) with spiral readout. Magn. Reson. Med. 2015;74:1621–1631 doi: 10.1002/mrm.25559.

10. Sbrizzi A, Heide O van der, Cloos M, et al. Fast quantitative MRI as a nonlinear tomography problem. Magn. Reson. Imaging 2018;46:56–63 doi: 10.1016/j.mri.2017.10.015.

11. Welsch GH, Scheffler K, Mamisch TC, et al. Rapid estimation of cartilage T2 based on double echo at steady state (DESS) with 3 Tesla. Magn. Reson. Med. 2009;62:544–549 doi: 10.1002/mrm.22036.

12. Heule R, Ganter C, Bieri O. Triple echo steady-state (TESS) relaxometry. Magn. Reson. Med. 2014;71:230–237 doi: 10.1002/mrm.24659.

13. de Rochefort L. Method and device for imaging by magnetic resonance. 2016:WO 2016/180947 A1.

14. de Rochefort L. Encoding with Radiofrequency Spoiling, Equilibrium States and Inverse Problem for Parametric Mapping. In: Proc. Intl. Soc. Mag. Reson. Med. 23. ; 2015. p. 445.

15. Leroi L, Coste A, de Rochefort L, et al. Simultaneous multi-parametric mapping of total sodium concentration, T1, T2 and ADC at 7 T using a multi-contrast unbalanced SSFP. Magn. Reson. Imaging 2018;53:156–163 doi: 10.1016/j.mri.2018.07.012.

16. Trattnig S, Springer E, Bogner W, et al. Key clinical benefits of neuroimaging at 7T. NeuroImage 2018;168:477–489 doi: 10.1016/j.neuroimage.2016.11.031.

17. Ladd ME, Bachert P, Meyerspeer M, et al. Pros and cons of ultra-high-field MRI/MRS for human application. Prog. Nucl. Magn. Reson. Spectrosc. 2018;109:1–50 doi: 10.1016/j.pnmrs.2018.06.001.

18. Kraff O, Quick HH. 7T: Physics, safety, and potential clinical applications. J. Magn. Reson. Imaging 2017;46:1573–1589 doi: 10.1002/jmri.25723.

19. van der Kolk AG, Hendrikse J, Zwanenburg JJM, Visser F, Luijten PR. Clinical applications of 7 T MRI in the brain. Eur. J. Radiol. 2013;82:708–718 doi: 10.1016/j.ejrad.2011.07.007.

20. Moser E, Stahlberg F, Ladd ME, Trattnig S. 7-T MR—from research to clinical applications? NMR Biomed. 2012;25:695–716 doi: 10.1002/nbm.1794.

21. Sullivan DC, Obuchowski NA, Kessler LG, et al. Metrology Standards for Quantitative Imaging Biomarkers. Radiology 2015;277:813–825 doi: 10.1148/radiol.2015142202.

22. Cloos MA, Knoll F, Zhao T, et al. Multiparametric imaging with heterogeneous radiofrequency fields. Nat. Commun. 2016;7:12445 doi: 10.1038/ncomms12445.

23. Neves AL, Leroi L, Raolison Z, et al. Compressed perovskite aqueous mixtures near their phase transitions show very high permittivities: New prospects for high-field MRI dielectric shimming. Magn. Reson. Med. 2018;79:1753–1765 doi: 10.1002/mrm.26771.

24. Dubois M, Leroi L, Raolison Z, et al. Kerker Effect in Ultrahigh-Field Magnetic Resonance Imaging. Phys. Rev. X 2018;8:031083 doi: 10.1103/PhysRevX.8.031083.

25. Cloos MA, Boulant N, Luong M, et al. kT -points: short three-dimensional tailored RF pulses for flip-angle homogenization over an extended volume. Magn. Reson. Med. 2012;67:72–80 doi: 10.1002/mrm.22978.

26. Gras V, Vignaud A, Amadon A, Le Bihan D, Boulant N. Universal pulses: A new concept for calibration-free parallel transmission. Magn. Reson. Med. 2017;77:635–643 doi: 10.1002/mrm.26148.

27. Pauly J, Roux PL, Nishimura D, Macovski A. Parameter relations for the Shinnar-Le Roux selective excitation pulse design algorithm. IEEE Trans. Med. Imaging 1991;10:53–65 doi: 10.1109/42.75611.

28. Roux PL, Hinks RS. Stabilization of echo amplitudes in FSE sequences. Magn. Reson. Med. 1993;30:183–190 doi: 10.1002/mrm.1910300206.

29. Scheffler K. A pictorial description of steady-states in rapid magnetic resonance imaging. Concepts Magn. Reson. 1999;11:291–304 doi: 10.1002/(SICI)1099-0534(1999)11:5<291::AID-CMR2>3.0.CO;2-J.

30. Kaiser R, Bartholdi E, Ernst RR. Diffusion and field-gradient effects in NMR Fourier spectroscopy. J. Chem. Phys. 1974;60:2966–2979 doi: 10.1063/1.1681477.

31. Freed DE, Scheven UM, Zielinski LJ, Sen PN, Hürlimann MD. Steady-state free precession experiments and exact treatment of diffusion in a uniform gradient. J. Chem. Phys. 2001;115:4249–4258 doi: 10.1063/1.1389859.

32. Helenius J, Soinne L, Perkiö J, et al. Diffusion-Weighted MR Imaging in Normal Human Brains in Various Age Groups. Am. J. Neuroradiol. 2002;23:194–199.

33. Haselgrove J, Prammer M. An algorithm for compensation of surface-coil images for sensitivity of the surface coil. Magn. Reson. Imaging 1986;4:469–472 doi: 10.1016/0730-725X(86)90024-X.

34. Valabrègue R, de Rochefort L. Fisher Information Matrix for Optimizing the Acquisition Parameters in Multi-Parametric Mapping Based on Fast Steady-State Sequences. In: Proc. Intl. Soc. Mag. Reson. Med. 24. ; 2016. p. 1569.

35. Wang R, Wang G-J, Goldstein RZ, et al. Induced magnetic force in human heads exposed to 4 T MRI. J. Magn. Reson. Imaging 2010;31:815–820 doi: 10.1002/jmri.22125.

36. Marques JP, Norris DG. How to choose the right MR sequence for your research question at 7T and above? NeuroImage 2018;168:119–140 doi: 10.1016/j.neuroimage.2017.04.044.

37. Marty B. Développements de stratégies de quantification et de dispositifs expérimentaux pour l'IRM moléculaire de biomarqueurs endovasculaires et intratissulaires de pathologies cérébrales [thesis]. Paris 11; 2012.

38. Preibisch C, Deichmann R. Influence of RF spoiling on the stability and accuracy of T1 mapping based on spoiled FLASH with varying flip angles. Magn. Reson. Med. 2009;61:125–135 doi: 10.1002/mrm.21776.

39. Yarnykh VL. Actual flip-angle imaging in the pulsed steady state: A method for rapid three-dimensional mapping of the transmitted radiofrequency field. Magn. Reson. Med. 2007;57:192–200 doi: 10.1002/mrm.21120.

40. Amadon A, Boulant N. Simultaneous measurement of B0- and B1-maps with modified Actual Flip Angle Imaging sequence. In: Proc. Intl. Soc. Mag. Reson. Med. ; 2008.

41. Gras V, Boland M, Vignaud A, et al. Homogeneous non-selective and slice-selective parallel-transmit excitations at 7 Tesla with universal pulses: A validation study on two commercial RF coils. PLOS ONE 2017;12:e0183562 doi: 10.1371/journal.pone.0183562.

42. Boulant N, Gras V, Amadon A, Luong M, Ferrand G, Vignaud A. Workflow proposal for defining SAR safety margins in parallel transmission. In: Proc. Intl. Soc. Mag. Reson. Med. 26. ; 2018. p. 295.

43. Tustison NJ, Cook PA, Klein A, et al. Large-scale evaluation of ANTs and FreeSurfer cortical thickness measurements. NeuroImage 2014;99:166–179 doi: 10.1016/j.neuroimage.2014.05.044.

44. Marcus DS, Wang TH, Parker J, Csernansky JG, Morris JC, Buckner RL. Open Access Series of Imaging Studies (OASIS): Cross-sectional MRI Data in Young, Middle Aged, Nondemented, and Demented Older Adults. J. Cogn. Neurosci. 2007;19:1498–1507 doi: 10.1162/jocn.2007.19.9.1498.

45. Rydberg JN, Riederer SJ, Rydberg CH, Jack CR. Contrast optimization of fluid-attenuated inversion recovery (FLAIR) imaging. Magn. Reson. Med. 1995;34:868–877.

46. Helms G. A precise and user-independent quantification technique for regional comparison of single volume proton MR spectroscopy of the human brain. NMR Biomed. 2000;13:398–406 doi: 10.1002/1099-1492(200011)13:7<398::AID-NBM660>3.0.CO;2-W.

47. Malik SJ, Teixeira RPAG, Hajnal JV. Extended phase graph formalism for systems with magnetization transfer and exchange. Magn. Reson. Med. 2018;80:767–779 doi: 10.1002/mrm.27040.

48. van Gelderen P, Jiang X, Duyn JH. Effects of Magnetization Transfer on T1 Contrast in Human Brain White Matter. NeuroImage 2016;128:85–95 doi: 10.1016/j.neuroimage.2015.12.032.

49. Hilbert T, Kober T, Zhao T, et al. Mitigating the Effect of Magnetization Transfer in Magnetic Resonance Fingerprinting. In: Proc. Intl. Soc. Mag. Reson. Med. 25. ; 2017. p. 74.

50. Boulant N. T1 and T2 effects during radio-frequency pulses in spoiled gradient echo sequences. J. Magn. Reson. 2009;197:213–218 doi: 10.1016/j.jmr.2008.12.023.

51. Dieringer MA, Deimling M, Santoro D, et al. Rapid Parametric Mapping of the Longitudinal Relaxation Time T1 Using Two-Dimensional Variable Flip Angle Magnetic Resonance Imaging at 1.5 Tesla, 3 Tesla, and 7 Tesla. PLOS ONE 2014;9:e91318 doi: 10.1371/journal.pone.0091318.

52. De Guio F, Vignaud A, Chabriat H, Jouvent E. Different types of white matter hyperintensities in CADASIL: Insights from 7-Tesla MRI. J. Cereb. Blood Flow Metab. 2018;38:1654–1663 doi: 10.1177/0271678X17690164.

53. Boada FE, Shen GX, Chang SY, Thulborn KR. Spectrally weighted twisted projection imaging: Reducing T2 signal attenuation effects in fast three-dimensional sodium imaging. Magn. Reson. Med. 1997;38:1022–1028 doi: 10.1002/mrm.1910380624.